HHS Public Access

Author manuscript

ACS ES T Water. Author manuscript; available in PMC 2022 July 11.

Published in final edited form as:

ACS ES T Water. 2022 May 13; 2(5): 863–872. doi:10.1021/acsestwater.2c00043.

Dual-Functional Nanofiltration and Adsorptive Membranes for PFAS and Organics Separation from Water

Francisco Léniz-Pizarro,
Department of Chemical and Materials Engineering, University of Kentucky, Lexington, Kentucky 40506, United States

Ronald J. Vogler,
Department of Chemical and Materials Engineering, University of Kentucky, Lexington, Kentucky 40506, United States

Phillip Sandman,
Department of Chemical and Materials Engineering, University of Kentucky, Lexington, Kentucky 40506, United States

Natalie Harris,
Department of Chemical and Materials Engineering, University of Kentucky, Lexington, Kentucky 40506, United States

Lindell E. Ormsbee,
Department of Civil Engineering, University of Kentucky, Lexington, Kentucky 40506, United States

Chunqing Liu,
Membranes R&D Group, Honeywell UOP, Des Plaines, Illinois 60016, United States

Dibakar Bhattacharyya
Department of Chemical and Materials Engineering, University of Kentucky, Lexington, Kentucky 40506, United States; Phone: 859-312-7790

Abstract

Challenges associated with water separation technologies for per- and polyfluoroalkyl substances (PFASs) require efficient and sustainable processes supported by a proper understanding of the separation mechanisms. The solute rejections by nanofiltration (NF) at pH values near the membrane isoelectric point were compared to the size- and mass-transfer-dependent modeled rejection rates of these compounds in an ionized state. We find that the low pK_a value of

Corresponding Author: **Dibakar Bhattacharyya** – Department of Chemical and Materials Engineering, University of Kentucky, Lexington, Kentucky 40506, United States; Phone: 859-312-7790; db@uky.edu.

Complete contact information is available at: https://pubs.acs.org/10.1021/acsestwater.2c00043

Supporting Information

The Supporting Information is available free of charge at https://pubs.acs.org/doi/10.1021/acsestwater.2c00043.
More details about the materials, the description of the methods used for characterization, analytical, and performance measurements; calculation of parameters, data processing, more ionogenic organics separation results; description and calculation for the models used; complementary material characterization (PDF)

The authors declare no competing financial interest.

perfluorooctanoic acid (PFOA) relates to enhanced solute exclusions by minimizing the presence and partitioning of the protonated organic compound into the membrane domain. The effects of Donnan exclusion are moderate, and co-ion transport also contributes to the PFAS rejection rates. An additional support barrier with thermo-responsive (quantified by water permeance variation) adsorption/desorption properties allows for enhanced separations of PFAS. This was possible by successfully synthesizing an NF layer on top of a poly-N-isopropylacrylamide (PNIPAm) pore-functionalized microfiltration support structure. The support layer adsorbs organics (178 mg PFOA adsorbed/m^2 membrane at an equilibrium concentration of 70 mg/L), and the simultaneous exclusion from the NF layer allows separations of PFOA and the smaller sized heptafluorobutyric acid from solutions containing 70 μg/L of these compounds at a high water flux of 100 L/m^2-h at 7 bar.

Graphical Abstract

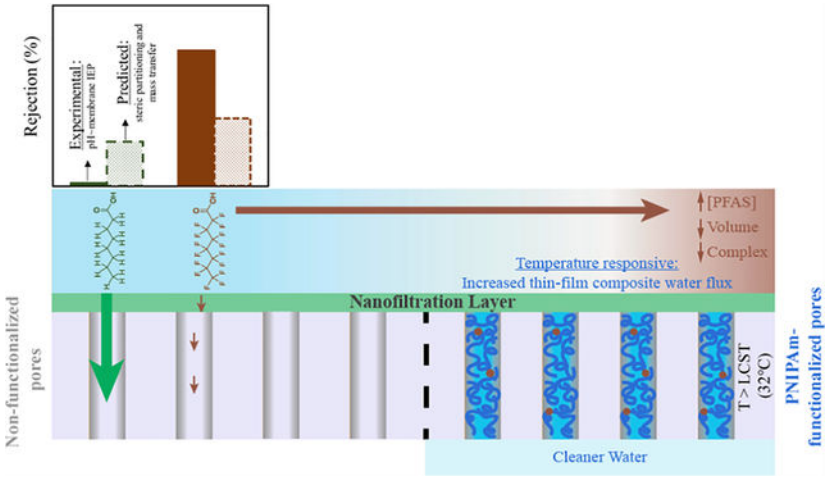

Keywords

PFAS; organic anions; water treatment; responsive materials

1. INTRODUCTION

Per- and polyfluoroalkyl substances (PFASs) have been a major focus of interest since these compounds are ubiquitous[1–4] and have concerning health effects.[5–7] Some of the most commonly studied PFAS compounds are perfluorooctanoic acid (PFOA) and perfluorooctane sulfonic acid (PFOS)[8] and more recently hexafluoropropylene oxide dimer acid (HFPO-DA, also referred to as GenX, DuPont's substitution for PFOA).[9] These compounds differ from some nontoxic compounds mainly because fluorine is included in their chemical structure instead of hydrogen. The electronegativity of the fluoroalkyl results in interesting intermolecular and intramolecular properties,[10] for example, acting as good surfactants,[11] being good oxygen carriers,[12] among others. A good understanding of these unique properties, as well as the similitudes they share with other organic compounds, can help improve the separation mechanisms for their removal from water bodies.

Currently, activated carbon (AC), ion exchange (IX) resins,[13] and membranes are the main technologies used to separate PFASs from water.[14] While the primary focus of these technologies has been to meet current EPA or state regulatory standards associated with drinking water (e.g., 70 ppt),[15] the handling of the captured PFAS presents an additional problem. Powdered activated carbon (PAC), which serves as a good adsorption technology for PFOA (277 mg/g),[16,17] has proven less efficient for adsorbing short-chain PFAS,[17,18] with removal efficiency around 20% for ~100 ppt perfluoropentanoic acid.[19] Furthermore, PAC must be regenerated through thermal reactivation.[8] A main environmental concern from thermal reactivation is the generation of fluorinated byproducts, for example, 8–13% of the decomposition products from PFOA and PFOS at pyrolysis conditions are not fully mineralized.[20–22] The release of these smaller sized generated fluorinated compounds can thus become a new contamination issue if not treated properly after the regeneration process.[8] The use of IX resins requires high capacity and post-regeneration. Sodium hydroxide–methanol mixtures are needed to obtain high regeneration yields[23] and are not necessarily designed for producing concentrated desorbed solutions. This causes a new waste management issue in which a more complicated mixture is generated.[8] On the other hand, polyamide thin-film composites such as nanofiltration (NF) and reverse osmosis (RO) membranes function under a different separation mechanism.[24–26] These membranes partially exclude PFAS regardless of their chain lengths and let water pass through, with the consequent formation of a more concentrated solution and a clean permeate stream. “Loose” polyamide thin-film composites also offer a less energy-intensive process relative to RO.[27] The generation of concentrated and easy-to-handle aqueous solutions of PFAS can provide new opportunities to move toward a zero-waste discharge alternative by potentially coupling the technology with PFAS destruction techniques.[8,28–31]

Polymeric microfiltration (MF) membranes have the capability of holding materials within their pores, supporting additional functionalities and providing an increased surface area for interactions. These characteristics allow for the introduction of metals and charged molecules,[32,33] grafted molecules,[34] and scaffolds for physical immobilization[32,35,36] for applications such as catalysis, adsorption, and the development of responsive materials. The separation of PFAS and other pollutants from contaminated water sources has also been studied.[35,37] Successful coupling of a polyamide thin-film layer on top of a functionalized open support presents some intriguing opportunities to create a single-step process, which concentrates and further purifies PFASs from an aqueous solution with a minimum decrease of the membrane water permeance. To the best of our knowledge, this has not been achieved yet because the synthesis of a polyamide layer on top of an open structure remains a challenge. Interfacial polymerization reactions[38,39] are further restricted by hydrophobic interactions in MF membranes such as poly(vinylidene fluoride) (PVDF), which reduces the liquid entry pressure of the organic phase.

This study focuses on (1) understanding the separation of environmentally relevant ionogenic organics, such as PFASs, by the exclusion mechanisms associated with NF membranes by using commercially available NF270 membranes, (2) the synthesis of polyamide thin film on top of a temperature-responsive and an open porous support that combines the benefits of the exclusion mechanism of NF membranes with adsorption, and

(3) the application of such composite membranes to the study of PFAS separation leading to a more sustainable water treatment solution.

2. MATERIALS AND METHODS

2.1. Materials and Chemicals.

The details of the chemicals used and some of their properties are listed in Tables S1 and S2.

2.2. Pore Functionalization and Synthesis of Polyamide Films.

To achieve the synthesis of a polyamide thin-film membrane on top of an open polymeric structure, a two-step process was implemented, as described in Figure 1. First, a commercial MF membrane PVDF400 was used as a porous support structure, on which an in-pore polymerization was performed similarly as described in previous work.[35] The poly-N-isopropylacrylamide (PNIPAm) mass gain was adjusted (Figure S1) to minimize defects on the PNIPAm-PVDF created support. At this synthesis stage, the pores decreased in size and obtained their temperature-responsive functionality. For the synthesis of the polyamide top layer, a piperazine-trimesoyl chloride interfacial polymerization reaction was used, as detailed in our previous work.[40] Thus, a nonporous NF-PNIPAm-PVDF thin-film composite was created.

2.3. Materials Characterization.

The surface morphologies of the porous support structures and the polyamide film were evaluated using a field emission scanning electron microscope (FESEM) (FEI Helios Nanolab 660). A K-alpha X-ray Photoelectron Spectroscopy (XPS) from Thermo Scientific was used for measuring the atomic composition of both the surface and the depth profile. More details on these techniques are provided in the Supporting Information. Hydrophobicity was studied by measuring the water contact angle using a drop shape analyzer, Kruss DSA100, by the sessile drop technique.

2.4. Separation Performance Experiments.

The transport of solutes and water through the polyamide thin-film composite and the porous structures were studied under convective and nonconvective (diffusive) processes. For solutions containing contaminants, such as PFAS, and other organic compounds for analogous studies, a small-volume continuous crossflow membrane testing unit was created (see Figure S2) on which two membranes were tested simultaneously. The thermo-responsiveness and performance testing of the porous supports and the thin-film composites were studied using a Sterlitech Membrane Test Cell System (WA) with four simultaneous cells and a larger processing capacity.[40] All samples were taken after 3 h of stabilization. The solutes permeabilities through NF membranes were tested in a diffusion cell under a concentration gradient and were modeled using the solution-diffusion equation $J_{solute} = B \cdot \Delta C$ (modeled as a reverse osmosis type membrane).[26] The solute permeability coefficient (B) under diffusive conditions was then calculated. An automated in-line ILC07 (PermeGear) system is explained in more detail in the Supporting Information, S1.4. Adsorption experiments were run in batch mode, primarily on a temperature-controlled shaker. Complimentarily studies were also run in a stirred (~300 rpm) flow through

dead-end cell Sterlitech HP4750. Details of the commercial and previously synthesized membranes are presented in Table S3.

2.5. Analytical Methods: LC-MS/MS, ICP-MS, TOC, UV–Vis, and Conductivity.

PFAS compounds were measured using a Shimadzu chromatograph (Model: LC-20 AD) equipped with a SIL 20 AC HT autosampler that was interfaced with electrospray ionization (ESI) from an AB SCIEX Flash Quant mass spectrometer (MS/MS) (Model: 4000QTRAP) and a Macherey Nagel analytical column. For the analysis of sodium, chloride, and calcium ions, an inductively coupled plasma mass spectrometer (ICP-MS) from Agilent (7800) was used. For most of the non-PFAS organic compounds, a total organic carbon analyzer (TOC-5000A) from Shimadzu was used. For measuring 2,4,6 trichlorophenol (2,4,6 TCP) and methylene blue, a UV–vis spectrometer (VWR UV-6300PC) was used, with a 292[41] and 664 nm wavelength, respectively. For completing the ion balance in solution, H^+ and OH^- were measured using a pH sensor. A conductivity meter Orion Star 212 from Thermo Scientific equipped with DuraProbe 4-electrode conductivity cells was used for measuring single salt concentrations. Limits of detection and more information can be found in the Supporting Information.

3. RESULTS AND DISCUSSION

3.1. Separation Characteristics of Organic Ionogenic Compounds Through a Loose Polyamide Thin Film.

NF membranes are great candidates for sustainably separating PFAS from water. These membranes can be used to overcome technological limitations such as (1) maintaining high PFAS separation regardless of the chain size, (2) avoiding saturation of the membrane separation capacity, and (3) limiting the generation of hazardous mixtures. As shown in Figure S3, commercial DuPont NF270 membranes can concentrate the initial sample concentration five-fold, even at 400 ppm levels, while maintaining rejections rates as high as 90%. Researchers have thoroughly studied the transport mechanism of inorganic ions[24,25] where ions have a fixed charge and the membrane surface charge is a function of the pH.[42–44] The Donnan steric pore model with dielectric exclusion (DSPM-DE) has been broadly used to represent this transport. The main partitioning and mass-transfer equations (i.e., the extended Nernst–Planck equations) are presented in eqs 1 and 2.[40] Partitioning accounts for steric (considering the ion i and "pore size" of the membrane, ϕ_i), Donnan (charge, $\exp\left(-\frac{z_i F}{RT}\Delta\psi_D\right)$), and dielectric (Born solvation, $\exp\left(-\frac{\Delta W_i}{kT}\right)$) exclusions are presented in eq 1. Here, c_i is the ion concentration (mol/m^3), γ_i is the ion activity coefficient, z_i is the ion valence, F is the Faraday constant (C/mol), $\Delta\psi_D$ is the Donnan potential (V), R is the universal gas constant (J mol^{-1} K^{-1}), T is the temperature (K), ΔW is the Born solvation energy barrier (J), and k is the Boltzmann constant (J/K). The ion flux (mol m^{-2} s^{-1}) (J_i, eq 2) through the polyamide layer accounts for diffusive $\left(D_{i,p}\frac{dc_i}{dx}\right)$, electrical potential $\left(-\frac{z_i c_i D_{i,p}}{RT}F\frac{d\psi}{dx}\right)$, and convective coupling ($K_{i,c}c_i J_v$) transport, where $D_{i,p}$ is the ion-hindered diffusion coefficient (m^2/s), ψ is the electrical potential (V), x is the distance (m), $K_{i,c}$ is a hindrance convective factor, and J_v is the permeate volume flux (m/s). However, organic ions

that protonate and deprotonate as a function of the aqueous media pH add an extra layer of complexity and a predictive model for such a system currently does not exist.

Partitioning (eq 1)

$$\frac{\gamma_i(0^+)c_i(0^+)}{\gamma_i(0^-)c_i(0^-)} = \phi_i \cdot \exp\left(-\frac{z_i F}{RT}\Delta\psi_D\right) \cdot \exp\left(-\frac{\Delta W_i}{kT}\right) \quad (1)$$

Extended Nernst–Planck equation (eq 2)

$$j_i = -D_{i,p}\frac{\mathrm{d}c_i}{\mathrm{d}x} - \frac{z_i c_i D_{i,p}}{RT}F\frac{\mathrm{d}\psi}{\mathrm{d}x} + K_{i,c}c_i J_v \quad (2)$$

3.1.1. Size, Shape, and Ionization Aspects.—Unlike inorganic ions, the size of organic ionogenic compounds can differ dramatically between their length and width. A simple example to analyze is fatty acid. Particularly, volatile fatty acids (VFAs) have become of great interest in recent years due to their potential use as biochemical building blocks[45] for molecular structures. In this study, the experimental separation of model compounds at different pH conditions was explored using commercial DuPont NF270 membranes (Figure 2a–c). Figure 2a, which includes the membrane isoelectric point (IEP, ~3.6[46–49]) and molecules' pK_a for reference, shows how the increase in the chain length of the fatty acids (FAs) tested did not contribute to a decrease in the transport through the polyamide membrane. Zhu et al.[50,51] recently investigated VFA separation using a Dow NF-45 membrane, where the separation performance was also highly dependent on the solution pH. For the largest fatty acid tested in this study, octanoate, the rejection was as low as 0% when less than 50% of the species were protonated. When octanoate was fully deprotonated, octanoate rejection increased to 30% (corroborated in Figure S4). To prove that higher rejection of octanoate can be expected at higher pH (which is associated with a higher negatively charged surface[52]), the separation of octanoate was tested at pH 10, which resulted in a rejection rate of around 75% (Figure S4). The fact that the rejection of octanoate goes as low as 0% at lower pH, while the rejection of analogous anionic PFASs (Figure 2b) stays high, regardless of the chain length,[29,53,54] suggests that the shortest axis of the compound's structure contributes the most to the rejection, although the rejection can be shape-influenced. Figure 2d compares the largest distance of the narrowest axis of the molecules/ions tested, referred to in this study as the effective chemical structure diameter. Details in the calculation are shown in the Supporting Information and summarized in Table S5. For the linear molecules, the circumscribed circle to the triangular base of the tetrahedral geometry was used. Values for bare (nonhydrated) structures were at least 33% smaller than the pore size of the membrane.

To isolate the separation mechanisms involved in the process, the DSPM-DE was used and the charge and dielectric exclusion at the interface (eq 1) were annulled ($X_d = 0$, $\varepsilon_p = \varepsilon_{bulk}$). Therefore, the combination of size partitioning (using the effective chemical structure diameter) and the mass transfer through the polyamide domain (eq 2) was investigated. Details on the modeling are explained in our previous work,[40] and some additional data are

presented in the Supporting Information (Table S6). In Figure 2e, the modeled size- and mass-transfer-dependent rejections of compounds in an ionized state (considering Na^+ as the counterion) were compared against experimental results at the lowest pH tested (near the membrane IEP) where charge (Donnan) effects are expected to be minimal. For the case of PFOA, the modeled rejection accounted for up to 46% of the total separation, and an additional barrier not captured by the model brought the experimental rejection values up by 44%. However, for FAs and 2,4,6 TCP, an opposite effect was observed, where the experimental rejection rates were significantly below the modeled values for the ionized compounds. The experimental results for chloride resembled modeled rejections close to its ionic state. The exploration of charge and other exclusion mechanisms is therefore needed to explain the variation in experimental rejections from these similar effective size molecules.

3.1.2. Other Partitioning Effects: Charge and Hydrophobic/Hydrophilic Interactions.—The charge effects coming from the membrane's surface and solutes were studied to help understand additional or reduced contributions from the observed modeled rejection rates. A detailed discussion is presented in the Supporting Information, S3.6. The reduced PFOA rejection (Figure S7) by a PIP/PAH-PS35 NF membrane that is more positively charged than NF270,[40] in addition to the enhanced strong adsorbed PFOA found in the PIP/PAH-PS35 membrane (Figure S8), suggested that NF membranes that contain an increased number of amine groups in the surface will partition more PFOA and consequently have lower rejection. pH-dependent rejection results of multivalent organic and inorganic anions under different pH conditions (Figure S9) suggested that the high experimental rejection of PFOA and PFOS maintained at moderate pH values could not be related to Donnan partitioning effects alone.

Partitioning due to hydrophilic and hydrophobic interactions is not considered in the traditional DSPM-DE and they affect the partitioning of the organic ionogenic compounds into the membrane domain, particularly for the cases where the organic compounds start protonating before the membrane surface (i.e., when pK_a > IEP). For example, 2,4,6 TCP is a molecule that has a strong interaction with the RO membranes when nonionized,[55] reducing the experimental rejections as observed when compared to the modeled ionized compounds in Figure 2e. These interactions can also be correlated to the octanol–water partitioning coefficient, including the effect of pH (Figure S10). This parameter helped explain the exclusion trend observed for fatty acids (Figure 3a). The literature values for Kow and pK_a for PFAS, however, account for a large standard deviation, which makes this analysis nonconclusive.

3.1.3. Role of Counterions.—The transport of ions through NF membranes involves the ion and the counterion moving simultaneously across the polymer to maintain the electroneutrality condition. Charge exclusion of co-ions is expected from eq 1 and this has been studied for the case of inorganic anions.[46] In Figure 2a–c, solutions contained H^+ or Na^+ as the main counterion depending on the solution pH and the molecule pK_a. Also, solute concentrations of 1 mM were equivalent to a H^+ concentration at pH ~3. Na^+ and H^+ are monovalent cations and can be compared by means of their steric exclusion effects. Results in Figure S11 show the expected decrease in the modeled rejections of

ionogenic compounds when H^+ is the counterion. The experimental concentrations of both the cations and the anions were monitored and some permeate concentrations are presented in Figure S12. The rejection of the ion and the counterion of NaCl and the FAs at their highest pH tested, thus containing Na^+ as the counterion, is presented in Figure 3a, and two main observations are discussed. First, the permeate samples were found in a 1:1 sodium:counterion ratio (within one standard deviation, Figure S13) according to the expected simultaneous transport of the cation and anion. Secondly, and of great significance, is how the sodium ion significantly varied its transport (i.e., its rejection) through the membrane depending on the anion in solution. Using this same principle, the transport of PFOS with Ca^{2+} has been found to increase the rejection by complexation.[56]

The present study also takes advantage of the electroneutrality condition[57] for measuring and validating the analytical detection of ionizable organic compounds from single solute aqueous solutions. An ICP-MS was used for measuring the sodium counterion of solutions made of the salt form of three anions (PFOA, octanoate, and Cl^-). Figure 3b shows how the electroneutrality condition translates to the analytical method by locating the concentrations of cations vs anions around the $x = y$ line, for both the synthetic feed solutions and the collected permeates, from easy-to-analyze NaCl to harder-to-analyze compounds such as perfluorooctanoate. Samples are introduced into the ICP-MS in a 2% nitric acid (~0.45 M) matrix, and consequently, at high H^+ concentration, it is expected to become the main counterion, while Na^+ ions become easily available for detection. The present analytical approach can offer theoretical detection limits of 59 ppt for sodium ions,[58] which translates to a theoretical detection limit of 1.1 ppb for perfluorooctanoate. In this study, the sodium detection limit obtained was around 300 ppt. Additionally, Figure S14 shows the immense benefit of the linear correlation between the measured Na^+ and PFOA concentrations from 23 ppb to 23 ppm, reducing sample preparation efforts needed (e.g., dilutions).

3.2. Toward Enhanced PFAS Separation.

3.2.1. Synthesis of a Polyamide Thin Film on Top of an Open Polymeric Structure.—

To obtain superior PFAS separation by taking advantage of the benefits offered by using NF membranes, and without compromising water permeance rates, a dual exclusion–adsorption platform is proposed (Figure 4a). A thin-film polyamide layer was successfully formed on top of an open porous structure, as described in Figure 1. Initially, the commercial porous PVDF400 was functionalized with PNIPAm, which has a lower critical solution temperature (LCST) of ~32 °C. At the LCST, the polymer experiences a conformation change,[59] collapsing chains and becoming more hydrophobic when transitioning to higher temperatures. This allows for thermo-responsiveness and potential temperature-swing PFAS adsorption/desorption. After synthesizing a top polyamide layer, the dual exclusion–adsorption platform was obtained. The PNIPAm incorporated into the PVDF pores turned the composite more hydrophilic (captured through contact angle measurements (Figure S15)), which was critical for allowing the interfacial polymerization reaction in the second synthesis step. An expected, water permeance decrease (Figure 4b), caused by the decrease of the pore size followed by the addition of a nonporous polyamide top layer from PVDF400 to NF-PNIPAm-PVDF, was observed. The transition of the morphology from a porous to a nonporous structure was well-captured through SEM

imaging (Figures 4c,d and S16). Similarly, the elemental composition observed through XPS analysis proved the addition of PNIPAm on the porous support along with the formation of a polyamide layer on the membrane surface. The presence of fluorine was the main indicator of the PVDF porous support structure. The presence of nitrogen and oxygen in Figure 4e revealed the addition of PNIPAm. The transition from an abundance of nitrogen and oxygen on the surface to a fluorine-dominated region, observed in Figure 4f, confirmed the synthesis of the NF membrane layer on top of the porous structure with PNIPAm. This approach, in which the pores are functionalized, brings immense opportunities for tailoring functionalities such as quaternary amine groups for higher PFAS adsorption capacity.

3.2.2. Separation Performance of the NF-PNIPAm-PVDF Composite.—The separation performance of the NF-PNIPAm-PVDF membrane was initially tested under convective flow using a neutral organic compound (such as sucrose) and inorganic salts (sodium sulfate and calcium chloride) (Figures S17 and S18). The results of the separation resembled a loose polyamide thin-film composite, in which the rejection of sucrose (~1 nm diameter) and Na_2SO_4 was close to 70%. As observed in Figure S16e, the 10 000× magnification SEM image of NF-PNIPAm-PVDF exposed a small section that contained a defect, which could also have contributed to the decreased rejection of sucrose and Na_2SO_4 relative to other NF membranes.

The separation of PFAS was measured in batch and continuous flow, with both pressure and concentration driving forces. The PFOA adsorption capability of the NF-PNIPAm-PVDF membrane was proved and compared against the control nonadsorptive NF270 membrane (Figure 5a). Besides enabling the construction of the NF layer on top of the open porous structure, PNIPAm provided faster adsorption of PFOA in batch adsorption and dead-end filtration modes, as observed in Figure S19a,b. A dynamic adsorption ratio (defined in the Supporting Information, S4.3) of 4.6 was found between the NF-PNIPAm-PVDF and the PVDF400 membranes after ~6 min of passing PFOA solutions in a dead-end mode. PNIPAm can also offer adsorption selectivity toward certain model hydrophobic compounds,[60] as was the case for methylene blue (Figure S20). At an equilibrium concentration (C_e) of 70 mg/L PFOA, the 178 mg/m^2 membrane was adsorbed (q_e) by the NF-PNIPAm-PVDF membrane, and 26% of the adsorption capacity was regenerated using water at T(22 °C) < LCST (Figure S21).

The overall retention of the PFAS compounds PFBA, GenX, and PFOA was tested using a crossflow system (Figure 5b). A total of 2 mM $CaCl_2$ was added into the solution as a potential complexation agent for enhancing PFAS separation by exclusion and for enhancing adsorption onto the PNIPAm due to the priming effect on the charged PFAS molecules.[61,62] The experimental temperature used was maintained above the PNIPAm LCST (36 °C) to favor the adsorption mechanism. Retentions at 12 h (~50% for PFBA and ~70% for PFOA and GenX) can be expected to come mainly from rejection effects; the initial adsorption phenomenon was not observed due to the standard deviation of the data obtained. By comparing Na_2SO_4 and PFOA rejections between the commercial NF270 and the present synthesized membranes (Figure 5b.2), it can be concluded that the decreased PFAS separation was due to the quality of the synthesized NF layer and increasing the density or minimizing the presence of defects would ensure higher PFAS

rejections. Convective flow results were validated with diffusive flow conditions (Figure 5c), with higher solute permeability coefficients (B) for PFOA and Na_2SO_4 observed for the NF-PNIPAm-PVDF relative to NF270 membranes. The diffusive transport of PFAS was positively correlated to the chain length of the compounds, as can be seen by the higher B values for PFBA compared to PFOA (Figure 5c.2). Figure S22 shows the diffusive flux from which B values were calculated, and Figure S23 includes the effect of $CaCl_2$ in solution and results from the NF270 membranes.

3.2.3. Thermo-Responsiveness.—The water permeance, also referred to as the water permeability coefficient (A), of the pore-functionalized PNIPAm-PVDF, the composite NF-PNIPAm-PVDF membrane, and the NF270 membrane as control were measured at different temperatures and corrected for the change in the viscosity of water due to the change in the temperature (as explained in the Supporting Information, S4.5). Figure 6a summarizes the calculated water permeance and Figure 6b shows the ratio of A (39 °C) over A (21 °C) after viscosity corrections. The NF270 membrane resembled the expected temperature independence of the viscosity-corrected water permeability, and the PNIPAm-PVDF membrane showed similar thermo-responsiveness behavior, as reported previously.[35] Surprisingly, the thermo-responsiveness was fully transferred toward the polyamide thin-film composite (NF-PNIPAm-PVDF). For this phenomenon to be possible, the porous support must have had a significant impact on the transport of water through the overall thin-film composite, as has been discussed in previous studies.[63–65] The support-layer water permeance could have a large impact on the water of the membrane if the selective NF layer had a comparable permeability or contained a significant number of defects. These two possible reasons were evaluated through a resistance model (Figure S24) similar to the one conducted by Werber et al.[66] A detailed discussion is presented in the Supporting Information, S4.5. The model results are presented in Figures S25 and S26 and Table S9. The minimal presence of visible defects on the NF-PNIPAm-PVDF membranes suggested the high influence of the temperature-responsive nature of the support on the observed water permeance of the NF-PNIPAm-PVDF could be driven by an NF layer permeability that is comparable to or higher than the support permeance. This leads to the possibility of having created an NF layer structure looser than commercial NF270 membranes.

4. CONCLUSIONS

We found that the separation of PFAS using NF membranes significantly differs from other ionogenic organics with similar effective diameters. FAs and 2,4,6 TCP, which have pK_a values > membrane IEP, experienced experimental rejections (near the membrane IEP) below the predicted rejection of their ionized form by contributions from size partitioning and mass-transfer (modeled). The reduced exclusion barrier was associated with hydrophobic interactions favoring partitioning of the organics. The experimental rejection of PFOA and PFOS, however, presented higher experimental rejection rates than the modeled values. Even though the effects of Donnan exclusion and counterion transport were proven to partially affect the rejection of PFAS, other main contributions that are not covered in this study were responsible for maintaining high PFAS rejection rates.

The synthesis of an NF layer on top of a PNIPAm pore-functionalized support structure combined the exclusion and adsorption mechanisms. Images from a scanning electron microscope and the analysis of the depth profile using X-ray photoelectron spectrometry validated the synthesis procedure. The temperature-responsive behavior of the PNIPAm was reflected in the water permeance of the thin-film composite with values ranging between 7 and 24 (L m^{-2} h^{-1}) per bar of pressure applied. A water-transport resistance model, used in conjunction with previous results, suggested that the NF layer formed on top of the open porous structure could be less dense than the thin film from typical commercial NF270 membranes.

The separation of PFAS using the dual exclusion–adsorption platform was tested under different modes. A batch adsorption study gave a value of q_e = 178 mg/m^2 membrane for PFOA when C_e = 70 mg/L, with 26% of the adsorption capacity regenerated (of 14.6 cm^2 sample area) using 20 mL of water at T (22 °C) < LCST. Additional results from a dead-end convective flow experiment suggested that PNIPAm sped up the dynamic adsorption capacity of the pore-functionalized platform. Also, PNIPAm allowed for selective adsorption of other model compounds such as methylene blue. The steady-state rejection of PFAS by NF-PNIPAm-PVDF membranes in a crossflow system for a feed solution containing 70 μg/L of each compound was ~70% for PFOA and GenX and ~50% for PFBA. The promising results obtained, combined with the synthesis of denser NF layers and tailored functionalization for adsorption, may lead to a more sustainable water treatment process for PFAS separation.

Supplementary Material

Refer to Web version on PubMed Central for supplementary material.

ACKNOWLEDGMENTS

Research reported in this publication was supported by the National Institute of Environmental Health Sciences of the National Institutes of Health under Award Number P42ES007380. The content is solely the responsibility of the authors and does not necessarily represent the official views of the National Institutes of Health. Partial support was also provided by Honeywell UOP. The authors would like to thank Dr. Andrew Morris, Dr. Abigail Burrows, Dr. Scott Stanley, and Michael Hedge for the time, assistance, and analytical support on LC-MS/MS analysis. Additionally, thanks to Benjamin Weaver and Solecta for providing technical expertise and the PVDF400 membranes. Also, thanks to Dr. Nicolas Briot for SEM assistance and Nicholas Cprek for helping to create the cross flow membrane testing unit.

REFERENCES

(1). Whitehead HD; Venier M; Wu Y; Eastman E; Urbanik S; Diamond ML; Shalin A; Schwartz-narbonne H; Bruton TA; Blum A; Wang Z; Green M; Tighe M; Wilkinson JT; Mcguinness S; Peaslee GF Fluorinated Compounds in North American Cosmetics. Environ. Sci. Technol. Lett 2021, 8, 538–544.

(2). Ellis DA; Martin JW; Silva AODE; Mabury AS; Hurley MD; Sulbaek Andersen PM; Wallington JT Degradation of Fluorotelomer Alcohols: A Likely Atmospheric Source of Perfluorinated Carboxylic Acids. Environ. Sci. Technol 2004, 38, 3316–3321. [PubMed: 15260330]

(3). Liu X; Guo Z; Folk EE IV; Roache NF Determination of fluorotelomer alcohols in selected consumer products and preliminary investigation of their fate in the indoor environment. Chemosphere 2015, 129, 81–86. [PubMed: 24997516]

(4). Ahrens L Polyfluoroalkyl compounds in the aquatic environment: a review of their occurrence and fate. J. Environ. Monit 2011, 13, 20–31. [PubMed: 21031178]

(5). Sunderland EM; Hu XC; Dassuncao C; Tokranov AK; Wagner CC; Allen JG A review of the pathways of human exposure to poly- and perfluoroalkyl substances (PFASs) and present understanding of health effects. J. Exposure Sci. Environ. Epidemiol 2019, 29, 131–147.

(6). Lohmann R; Cousins IT; Dewitt JC; Glüge J; Goldenman G; Herzke D; Lindstrom AB; Miller MF; Ng CA; Patton S; Scheringer M; Trier X; Wang Z Are Fluoropolymers Really of Low Concern for Human and Environmental Health and Separate from Other PFAS? Environ. Sci. Technol 2020, 54, 12820–12828. [PubMed: 33043667]

(7). Fenton SE; Ducatman A; Boobis A; Dewitt JC; Lau C; Ng C; Smith JS; Roberts SM Per- and Polyfluoroalkyl Substance Toxicity and Human Health Review: Current State of Knowledge and Strategies for Informing Future Research. Environ. Toxicol. Chem 2021, 40, 606–630. [PubMed: 33017053]

(8). Wanninayake DM Comparison of currently available PFAS remediation technologies in water: A review. J. Environ. Manage 2021, 283, No. 111977. [PubMed: 33517051]

(9). Cousins IT; Dewitt JC; Glüge J; Goldenman G; Herzke D; Lohmann R; Miller M; Ng CA; Scheringer M; Vierke L; Wang Z Strategies for grouping per- and polyfluoroalkyl substances (PFAS) to protect human and environmental health. Environ. Sci.: Processes Impacts 2020, 22, 1444–1460.

(10). O'Hagan D Understanding organofluorine chemistry. An introduction to the C – F bond. Chem. Soc. Rev 2008, 37, 308–312. [PubMed: 18197347]

(11). Costanza J; Arshadi M; Abriola LM; Pennell KD Accumulation of PFOA and PFOS at the Air – Water Interface. Environ. Sci. Technol. Lett 2019, 6, 487–491.

(12). Squires JE Artificial blood. Science 2002, 295, 1002–1005. [PubMed: 11834811]

(13). Zhang DQ; Zhang WL; Liang YN Science of the Total Environment Adsorption of perfluoroalkyl and polyfl uoroalkyl substances (PFASs) from aqueous solution - A review. Sci. Total Environ 2019, 694, No. 133606. [PubMed: 31401505]

(14). Jansen K "Forever chemicals" no more? These technologies aim to destroy PFAS in water Chem. Eng. News, 2019, 97, 28.

(15). Drinking Water Health Advisories for PFOA and PFOS https://www.epa.gov/ground-water-and-drinking-water/drinking-water-health-advisories-pfoa-and-pfos (accessed September 10, 2021).

(16). Yu Q; Zhang R; Deng S; Huang J; Yu G Sorption of perfluorooctane sulfonate and perfluorooctanoate on activated carbons and resin: Kinetic and isotherm study. Water Res 2009, 43, 1150–1158. [PubMed: 19095279]

(17). Gagliano E; Sgroi M; Falciglia PP; Vagliasindi FGA; Roccaro P Removal of poly- and perfluoroalkyl substances (PFAS) from water by adsorption: Role of PFAS chain length, effect of organic matter and challenges in adsorbent regeneration. Water Res 2020, 171, No. 115381. [PubMed: 31923761]

(18). Li F; Duan J; Tian S; Ji H; Zhu Y; Wei Z; Zhao D Short-chain per- and polyfl uoroalkyl substances in aquatic systems: Occurrence, impacts and treatment. Chem. Eng. J 2020, 380, No. 122506.

(19). Son H; Kim T; Yoom H; Zhao D; An B The Adsorption Selectivity of Short and Long Per- and Polyfluoroalkyl Substances (PFASs) from Surface Water Using Powder-Activated Carbon. Water 2020, 12, No. 3287.

(20). Krusic PJ; Marchione AA; Roe DC Gas-phase NMR studies of the thermolysis of perfluorooctanoic acid. J. Fluorine Chem 2005, 126, 1510–1516.

(21). Xiao F; Sasi PC; Yao B; Kubatova A; Golovko MY; Golovko SA; Soli D Thermal Stability and Decomposition of Perfluoroalkyl Substances on Spent Granular Activated Carbon. Environ. Sci. Technol 2020, 7, 343–350.

(22). Xiao F; Sasi PC; Alinezhad A; Golovko SA; Golovko MY; Spoto A Thermal Decomposition of Anionic, Zwitterionic, and Cationic Polyfluoroalkyl Substances in Aqueous Film-Forming Foams. Environ. Sci. Technol 2021, 55, 9885–9894. [PubMed: 34235932]

(23). Gao Y; Deng S; Du Z; Liu K; Yu G Adsorptive removal of emerging polyfluoroalky substances F-53B and PFOS by anion-exchange resin: A comparative study. J. Hazard. Mater 2017, 323, 550–557. [PubMed: 27184593]

(24). Bowen WR; Welfoot JS Modelling the performance of membrane nanofiltration-critical assessment and model development. Chem. Eng. Sci 2002, 57, 1121–1137.

(25). Bandini S; Vezzani D Nanofiltration modeling: The role of dielectric exclusion in membrane characterization. Chem. Eng. Sci 2003, 58, 3303–3326.

(26). Wijmans JG; Baker RW The solution-diffusion model: a review. J. Membr. Sci 1995, 107, 1–21.

(27). Zhao Y; Tong T; Wang X; Lin S; Reid EM; Chen Y Differentiating Solutes with Precise Nanofiltration for Next Generation Environmental Separations: A Review. Environ. Sci. Technol 2021, 55, 1359–1376. [PubMed: 33439001]

(28). Vecitis CD; Park H; Cheng J; Mader BT; Hoffmann MR Kinetics and Mechanism of the Sonolytic Conversion of the Aqueous Perfluorinated Surfactants, Perfluorooctanoate (PFOA), and Perfluorooctane Sulfonate (PFOS) into Inorganic Products. J. Phys. Chem. A 2008, 112, 4261–4270. [PubMed: 18447373]

(29). Soriano A; Schaefer C; Urtiaga A Enhanced treatment of perfluoroalkyl acids in groundwater by membrane separation and electrochemical oxidation. Chem. Eng. J. Adv 2020, 4, No. 100042.

(30). Horst J; McDonough J; Ross I; Houtz E Understanding and Managing the Potential By-Products of PFAS Destruction. Groundwater Monit. Rem 2020, 40, 17–27.

(31). Verma S; Varma RS; Nadagouda MN Remediation and mineralization processes for per- and polyfluoroalkyl substances (PFAS) in water: A review. Sci. Total Environ 2021, 794, No. 148987. [PubMed: 34426018]

(32). Wan H; Islam S; Briot NJ; Schnobrich M; Pacholik L; Ormsbee L; Bhattacharyya D Pd/Fe nanoparticle integrated PMAA-PVDF membranes for chloro-organic remediation from synthetic and site groundwater. J. Membr. Sci 2020, 594, No. 117454.

(33). Sarma R; Islaman MS; Miller A; Bhattacharyya D Layer-by-Layer-Assembled Laccase Enzyme on Stimuli-Responsive Membranes for Chloro-Organics Degradation. ACS Appl. Mater. Interfaces 2017, 9, 14858–14867. [PubMed: 28397501]

(34). Islam MS; Vogler RJ; Abdullah Al Hasnine SM; Hernandez S; Malekzadeh N; Hoelen TP; Hatakeyama ES; Bhattacharyya D Mercury removal from wastewater using cysteamine functionalized membranes. ACS Omega 2020, 5, 22255–22267. [PubMed: 32923783]

(35). Saad A; Mills R; Wan H; Mottaleb MA; Ormsbee L; Bhattacharyya D Thermo-responsive adsorption-desorption of perfluoroorganics from water using PNIPAm hydrogels and pore functionalized membranes. J. Membr. Sci 2020, 599, No. 117821.

(36). Jebur M; Sengupta A; Chiao Y; Kamaz M; Qian X; Wickramasinghe R Pi electron cloud mediated separation of aromatics using supported ionic liquid (SIL) membrane having antibacterial activity. J. Membr. Sci 2018, 556, 1–11.

(37). Saad A; Mills R; Wan H; Ormsbee L; Bhattacharyya D Thermoresponsive PNIPAm – PMMA-Functionalized PVDF Membranes with Reactive Fe – Pd Nanoparticles for PCB Degradation. Ind. Eng. Chem. Res 2020, 59, 16614–16625.

(38). Song Y; Fan J; Wang S Recent progress in interfacial polymerization. Mater. Chem. Front 2017, 1, 1028–1040.

(39). Paul M; Jons SD Chemistry and fabrication of polymeric nanofiltration membranes: A review. Polymer 2016, 103, 417–456.

(40). Léniz-Pizarro F; Liu C; Colburn A; Escobar IC; Bhattacharyya D Positively charged nanofiltration membrane synthesis, transport models, and lanthanides separation. J. Membr. Sci 2021, 620, No. 118973.

(41). Williams ME; Hestekin JA; Smothers CN; Bhattacharyya D Separation of organic pollutants by reverse osmosis and nanofiltration membranes: Mathematical models and experimental verification. Ind. Eng. Chem. Res 1999, 38, 3683–3695.

(42). Coronell O; Mariñas BJ; Zhang X; Cahill DG Quantification of functional groups and modeling of their ionization behavior in the active layer of FT30 reverse osmosis membrane. Environ. Sci. Technol 2008, 42, 5260–5266. [PubMed: 18754378]

(43). Luxbacher T The ZETA Guide – Principles of the Streaming Potential Technique, 1et ed.; Anton Paar GmbH: Graz, Austria, 2014.

(44). Déon S; Fievet P; Osman Doubad C Tangential streaming potential/current measurements for the characterization of composite membranes. J. Membr. Sci 2012, 423–424, 413–421.

(45). Atasoy M; Owusu-agyeman I; Plaza E; Cetecioglu Z Bio-based volatile fatty acid production and recovery from waste streams: Current status and future challenges. Bioresour. Technol 2018, 268, 773–786. [PubMed: 30030049]

(46). Epsztein R; Shaulsky E; Dizge N; Warsinger DM; Elimelech M Role of Ionic Charge Density in Donnan Exclusion of Monovalent Anions by Nanofiltration. Environ. Sci. Technol 2018, 52, 4108–4116. [PubMed: 29510032]

(47). Lin Y-L Effects of Physicochemical Properties of Nanofiltration Membranes on the Rejection of Small Organic DBP Precursors. J. Environ. Eng 2013, 139, 127–136.

(48). Semião AJ; Schäfer AI Estrogenic micropollutant adsorption dynamics onto nanofiltration membranes. J. Membr. Sci 2011, 381, 132–141.

(49). Oatley DL; Llenas L; Pérez R; Williams PM; Martínezlladó X; Rovira M Review of the dielectric properties of nanofiltration membranes and verification of the single oriented layer approximation. Adv. Colloid Interface Sci 2012, 173, 1–11. [PubMed: 22405540]

(50). Zhu Y; Galier S; Balmann HR Description of the variation of retention versus pH in nanofiltration of organic acids. J. Membr. Sci 2021, 637, No. 119588.

(51). Zhu Y; Galier S; de Balmann HR Nanofiltration of solutions containing organic and inorganic salts: Relationship between feed and permeate proportions. J. Membr. Sci 2020, 613, No. 118380.

(52). Ritt CL; Werber JR; Wang M; Yang Z; Zhao Y; Kulik HJ; Elimelech M Ionization behavior of nanoporous polyamide membranes. Proc. Natl. Acad. Sci. U.S.A 2020, 117, 30191–30200. [PubMed: 33184175]

(53). Li M; Sun F; Shang W; Zhang X; Dong W; Dong Z; Zhao S Removal mechanisms of perfluorinated compounds (PFCs) by nanofiltration: Roles of membrane-contaminant interactions. Chem. Eng. J 2021, 406, No. 126814.

(54). Steinle-Darling E; Reinhard M Nanofiltration for Trace Organic Contaminant Removal: Structure, Solution, and Membrane Fouling Effects on the Rejection of Perfluorochemicals. Environ. Sci. Technol 2008, 42, 5292–5297. [PubMed: 18754383]

(55). Soriano l.; Gorri D; Urtiaga A Selection of High Flux Membrane for the Effective Removal of Short-Chain Perfluorocarboxylic Acids. Ind. Eng. Chem. Res 2019, 58, 3329–3338.

(56). Zhao C; Zhang J; He G; Wang T; Hou D; Luan Z Perfluorooctane sulfonate removal by nanofiltration membrane the role of calcium ions. Chem. Eng. J 2013, 233, 224–232.

(57). MacGillivray AD Nernst-Planck Equations and the Electroneutrality and Donnan Equilibrium Assumptions. J. Chem. Phys 1968, 48, No. 2903.

(58). Wilbur S The Agilent 7700x/7800 ICP-MS Advantage for Drinking Water Analysis, Washington, USA, 2015. https://www.lqa.com/wp-content/uploads/2017/05/agilent-7800-appnote.pdf.

(59). Yim H; Kent MS; Mendez S; Balamurugan SS; Balamurugan S; Lopez GP; Satija S Temperature-Dependent Conformational Change of PNIPAM Grafted Chains at High Surface Density in Water. Macromolecules 2004, 37, 1994–1997.

(60). Xiao L; Isner AB; Hilt JZ; Bhattacharyya D Temperature Responsive Hydrogel with Reactive Nanoparticles. J. Appl. Polym. Sci 2013, 128, 1804–1814. [PubMed: 30518988]

(61). Wu Q; Wang R; Chen X; Ghosh R Temperature-responsive membrane for hydrophobic interaction based chromatographic separation of proteins in bind-and-elute mode. J. Membr. Sci 2014, 471, 56–64.

(62). Higgins CP; Luthy RG Sorption of Perfluorinated Surfactants on Sediments. Environ. Sci. Technol 2006, 40, 7251–7256. [PubMed: 17180974]

(63). Wijmans JG; Hao P Influence of the porous support on diffusion in composite membranes. J. Membr. Sci 2015, 494, 78–85.

(64). Hao P; Wijmans JG; He Z; White LS Effect of pore location and pore size of the support membrane on the permeance of composite membranes. J. Membr. Sci 2020, 594, No. 117465.

(65). Ghosh AK; Hoek EMV Impacts of support membrane structure and chemistry on polyamide – polysulfone interfacial composite membranes. J. Membr. Sci 2009, 336, 140–148.

(66). Werber JR; Porter CJ; Elimelech M A Path to Ultraselectivity: Support Layer Properties to Maximize Performance of Biomimetic Desalination Membranes. Environ. Sci. Technol 2018, 52, 10737–10747. [PubMed: 30106285]

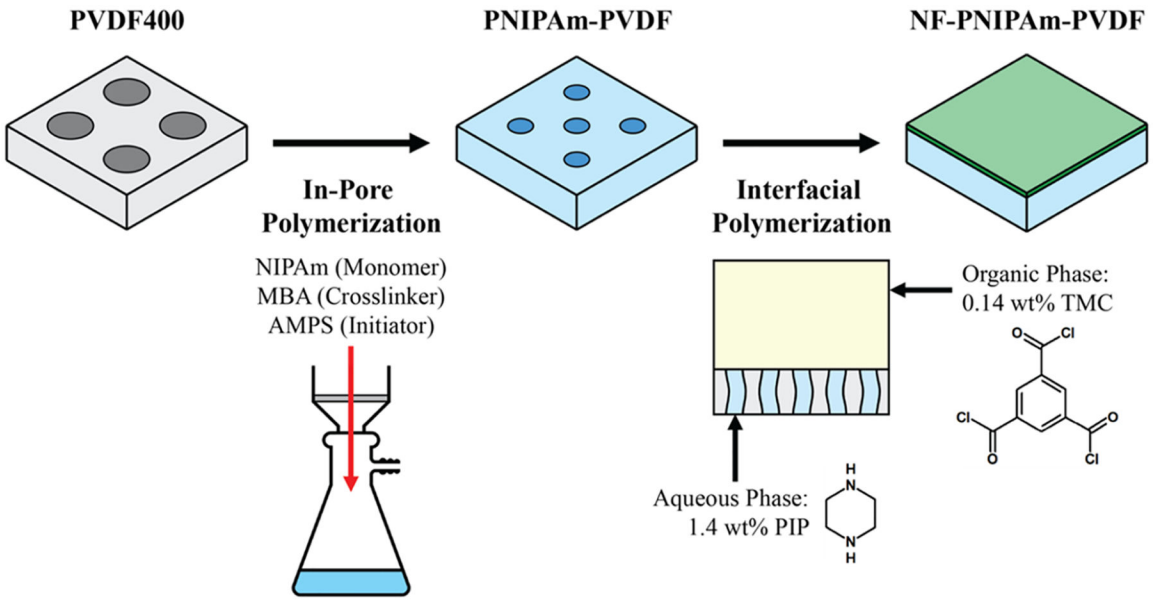

Figure 1.

Synthesis steps for the creation of a polyamide thin film on top of an open polymeric structure with pore functionality.

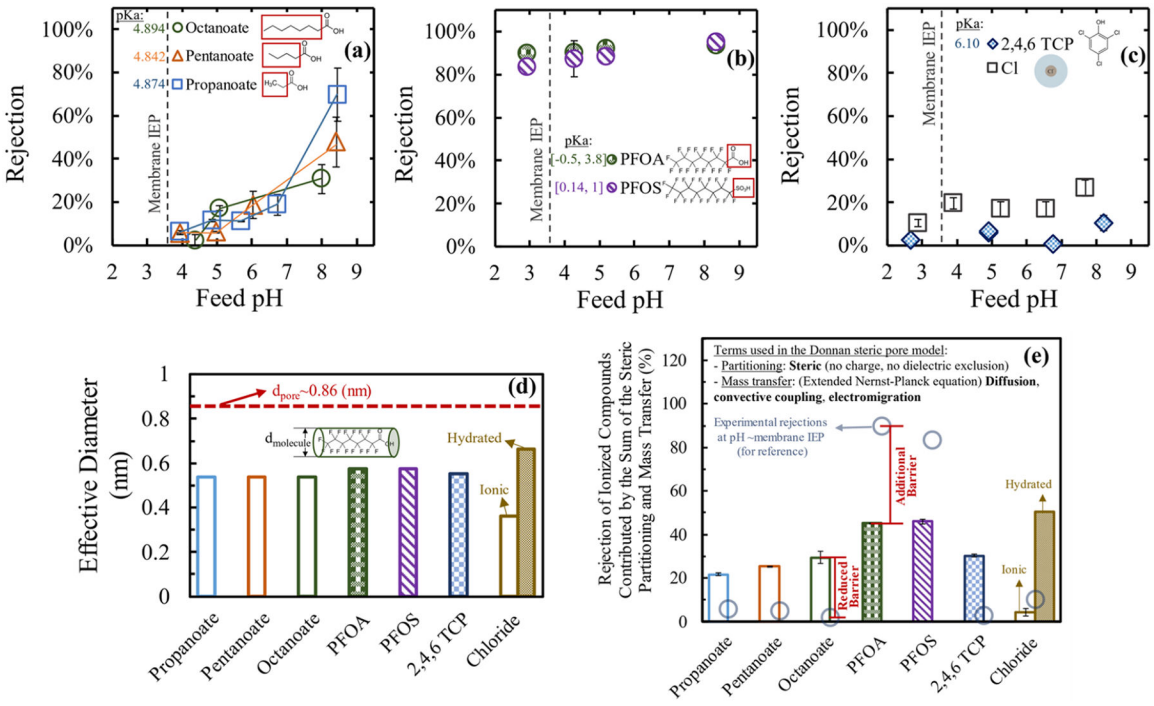

Figure 2.

Experimental (a–c) and modeled separation of ionogenic organic and inorganic ions using a commercial DuPont NF270 membrane. (a) Fatty acids of three different chain lengths (C8, C5, and C3) at 144.2, 160, and 148 ppm, respectively. (b) Fluorinated compounds with a backbone of 8 carbons and different functional groups (carboxylic acid (PFOA) and sulfonic acid (PFOS)). PFOA and PFOS (~160 ppm each) were run as a mixture. (c) Organic and inorganic symmetric anions: 2,4,6 trichlorophenol (2,4,6 TCP, ~165 ppm) and chloride coming from a NaCl ~59 ppm solution. Each compound/ion was measured directly by (a) TOC, (b) LC-MS/MS, and (c) UV–vis and ICP-MS. pH was modified either using NaOH to keep Na^+ as the main counterion or HCl. A crossflow membrane unit at 65 psi, 25 °C. Synthetic solutions were made in ASTM type 1 water. The isoelectric point (IEP) of the membrane and the electrolyte pK_a are indicated in each plot. (d) Critical distance (diameter) of molecules/ions tested compared to the modeled pore diameter of the DuPont NF270 membrane. In the case of PFOA, PFOS, and fatty acid tested, the critical distance or dimension was considered as the diameter of an imaginary cylinder formed by the molecule. Details on the calculation for molecules'/ions' critical dimension are presented in the Supporting Information and summarized in Table S5. (e) Comparison between the modeled steric and mass-transfer-related rejection of ionized solutes (colored bars) and the experimental rejections at pH ~ IEP (i.e., the lowest pH tested) (light blue circles). Some modeling parameters used were: $X_d = 0$, $\varepsilon_p = \varepsilon_{bulk}$, Na^+ as the counterion, $J_w = 65$ LMH, 0.5 mM of individual solutions, and $r_p = 0.43$ nm.

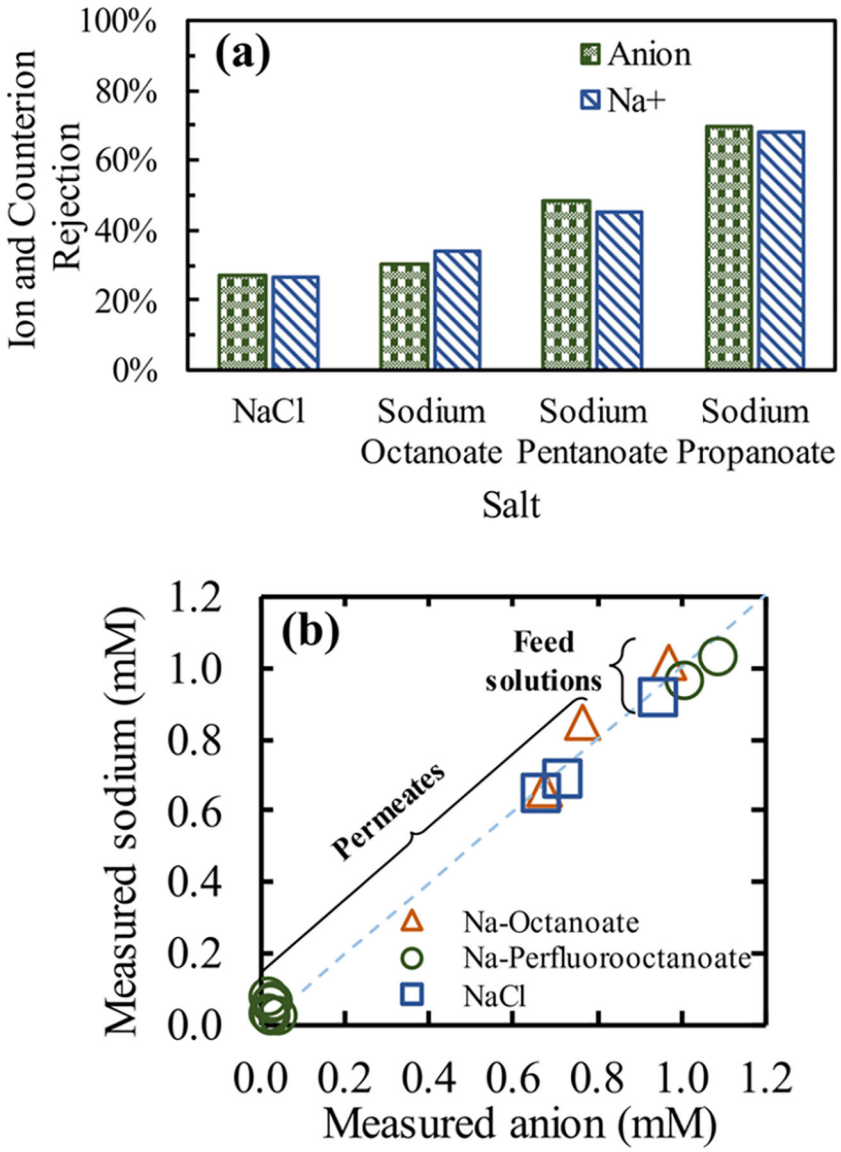

Figure 3.

Relevance of the counterion in the transport of organic anions through an NF membrane. (a) Rejection of the cation and the anion after separation using commercial DuPont NF270 membranes, corresponding to the highest pH tested from the respective anion from Figure 2, thus ensuring Na^+ as the main counterion. The different anions in solution influenced the Na^+ retention. (b) Translation of the electroneutrality condition on the single solute feed and permeate samples from filtration experiments toward analytical techniques. 1:1 cation/anion analytical detection for sodium octanoate, sodium perfluorooctanoate, and sodium chloride solutions (no pH modification). Sodium was measured using ICP-MS, Octanoate was measured using TOC, perfluorooctanoate was measured using LC-MS/MS, and chloride was measured using ICP-MS.

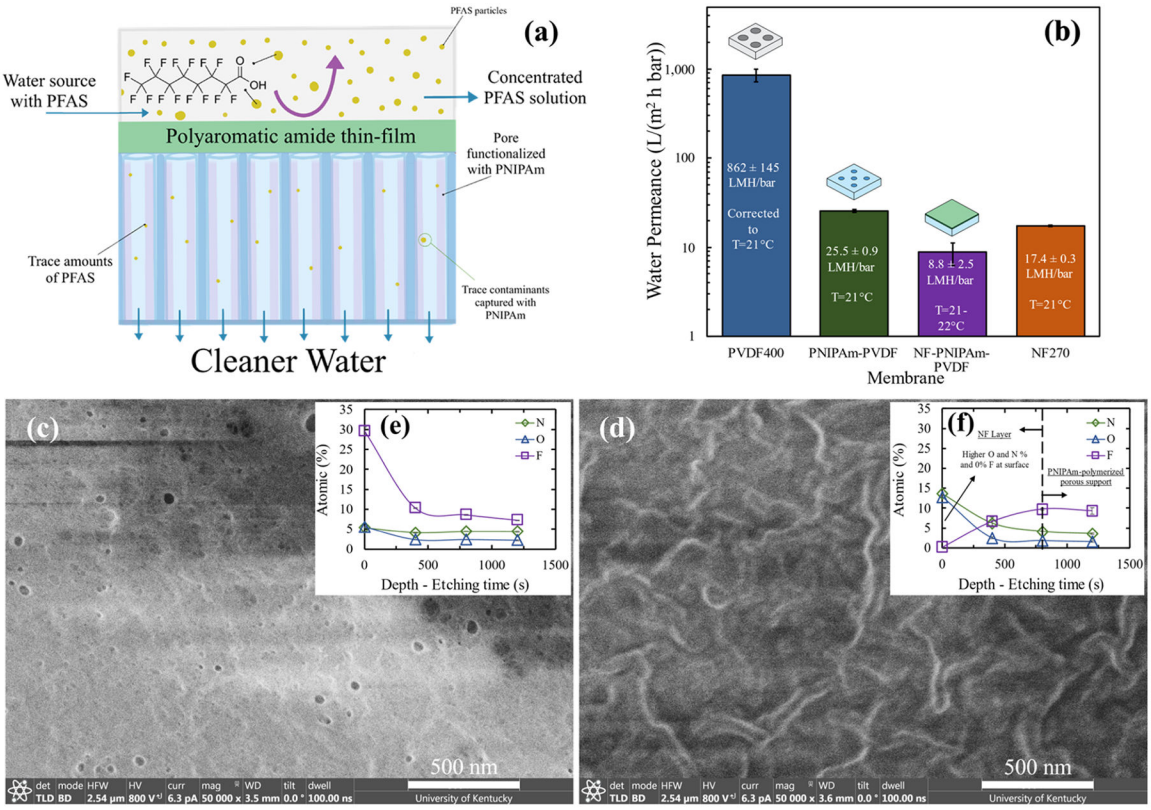

Figure 4.

(a) Diagram illustrating the developed material and its separation mechanisms (exclusion and adsorption) toward PFAS separation. (b) Water permeability coefficient (A) or also called water permeance (thickness-dependent) of the commercial PVDF400, PNIPAm-PVDF (weight gain 14.8%), and NF-PNIPAm-PVDF membranes (PNIPAm weight gain 10.0–11.7%) was calculated from the equation $J_w = A \cdot (\Delta P)$. Data for NF270 was included for comparison. The permeability was measured over a pressure range of 1.4–4.0 bar for the PVDF400 membrane, 1.9–9.2 bar for the PNIPAm-PVDF and NF270 membranes, and 2.0–9.6 bar for the NF-PNIPAm-PVDF membrane. Crossflow systems were used for these measurements. For the membrane containing functional materials and the NF270 membrane, the measurements were taken at 21–22 °C; PVDF400 measurements were taken at 26 °C and adjusted to 21 °C using viscosity corrections. (c, d) SEM of the surface transformation from the (c) pore-functionalized material to the formation of the (d) thin-film polyamide. (e, f) XPS depth profiles of the respective materials from each SEM image to corroborate PNIPAm and polyamide addition. Carbon accounts for the remaining percent.

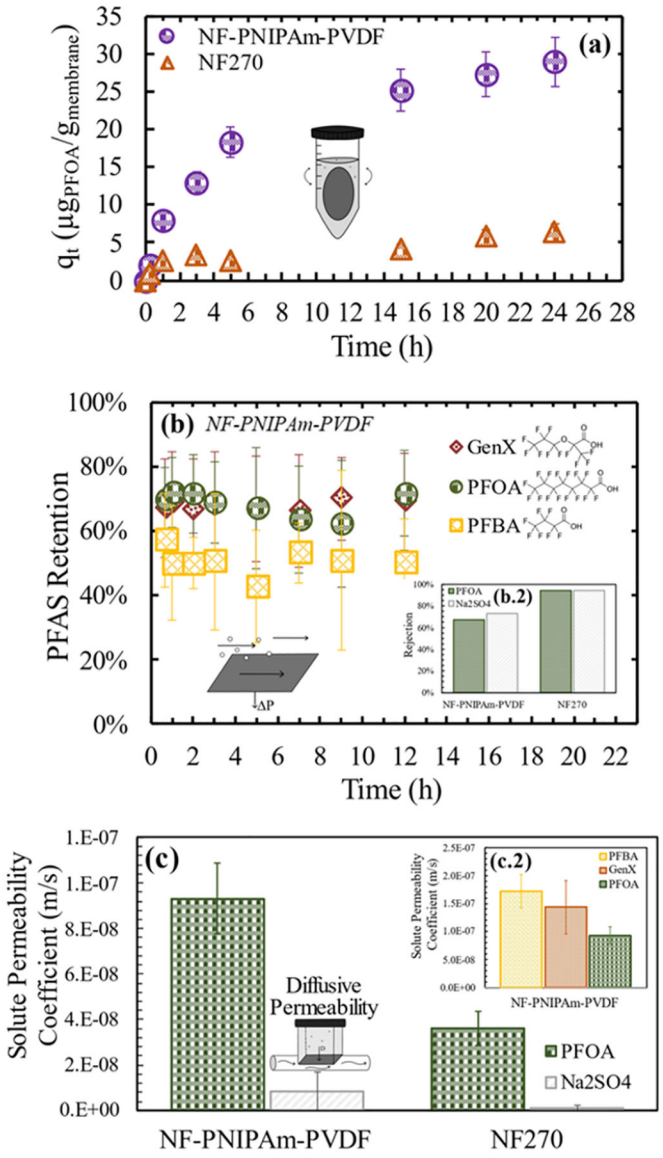

Figure 5.

PFAS separation under a diffusive and a convective flow. (a) PFOA adsorption over time in a batch mode. Membranes were set up in a 50 mL centrifuge tube, agitated in a shaking platform at 150 rpm, and the temperature was kept at 38 °C. Forty-eight milliliters of the initial volume of a solution with 130 ppb was initially fed. Membranes had a 14.6 cm^2 area, with approximate weights of 0.2 g. The NF-PNIPAm-PVDF membrane contained ~10% PNIPAm. Error bars represent the analytical error from measurements. (b) Retention of PFAS in a convective flow. Heptafluoropropylene oxide dimer acid (HFPO-DA) fluoride (GenX), perfluorooctanoic acid (PFOA), and heptafluorobutyric acid (PFBA) over time. Polymeric membranes were tested using two cells on a crossflow membrane unit and error bars represent the standard deviation between the two cells. T = 36 °C, pH ~5.7, and ~100 L/m^2-h at 7 bar permeate flux, 70 ppb of each PFAS, and 2 mM $CaCl_2$ as feed concentration. (b.2) Comparison of the rejection of PFOA and Na_2SO_4 between NF-PNIPAm-PVDF and

NF270. (c) Permeability coefficients of PFOA and Na_2SO_4 as an inorganic salt control, through NF membranes modeled as denser reverse osmosis membranes using the solution-diffusion equation for solute transport. The experiment was run in a constant driving force in-line diffusion system, at 37 °C, ~10 ppm concentration of each PFAS for starting feed concentrations in type I water over 12 h. (c.2) PFAS diffusive permeability coefficients through the NF-PNIPAm-PVDF membranes.

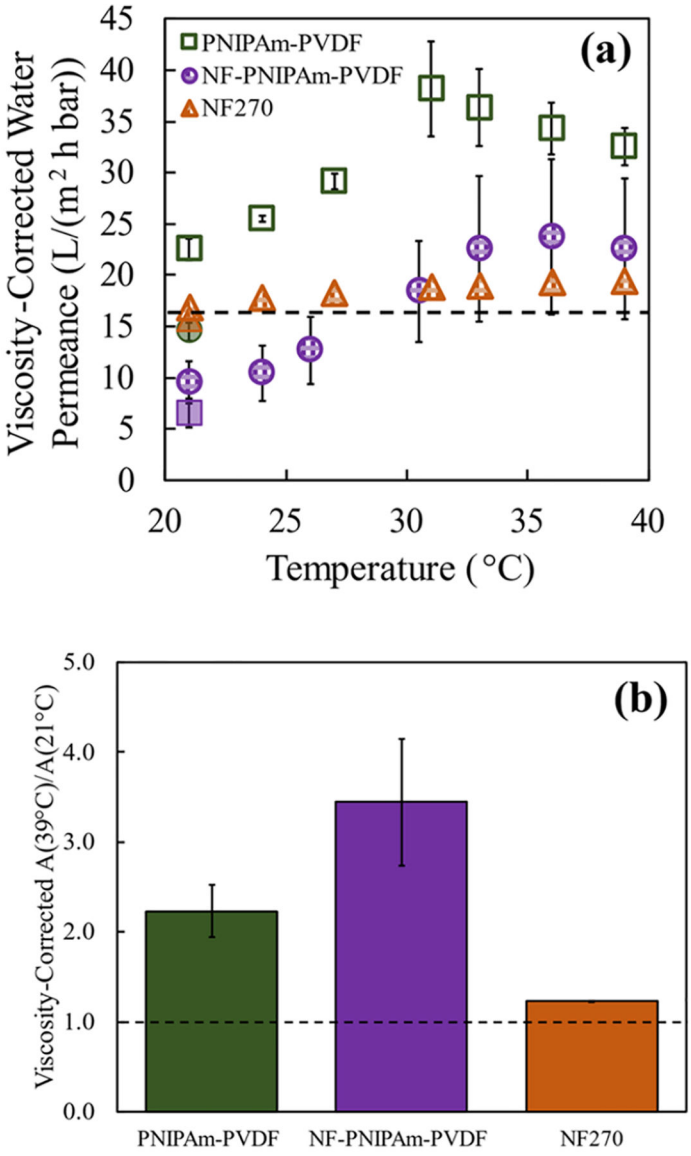

Figure 6.

Impact of the temperature on the viscosity-corrected water permeance of PNIPAm-synthesized membranes. The water permeability coefficient (A) or also called water permeance (thickness-dependent) was calculated from the equation $J_w = A \cdot (\Delta P)$ and then corrected for the effect of the temperature on the viscosity of water by normalizing to the viscosity at 21 °C. (a) Water permeance as a function of temperature for PNIPAm-PVDF (PNIPAm weight gain of 14.8%), NF-PNIPAm-PVDF (PNIPAm weight gain of 10.0–11.7%), and NF270 membranes. The temperature was increased from an initial value of 21–39 °C (hollow points) before being reset to 21 °C (shaded points). A crossflow unit was used for the measurements. (b) Ratios of the viscosity-corrected water permeability coefficient (A) at 39 °C to the water permeability (A) at 21 °C. The final permeability at 21 °C (shaded point) was used to calculate the permeability ratio.